ARTICLE

Solid polymorphism and dynamic magnetic properties of dodecylated vanadyl-porphyrinato complex: Spin-lattice relaxations modulated by phase stabilisation†

Received 00th January 20xx,
Accepted 00th January 20xx

DOI: 10.1039/x0xx00000x

Yoji Horii,*[a] Momo Makino,[a] Taro Yamamoto,[b] Shoichi Tatsumi,[b] Hal Suzuki,[b] Mariko Noguchi,[c] Takefumi Yoshida,[d] Takashi Kajiwara,[a] Zhao-Yang Li,[e] Masahiro Yamashita*[e,f]

The dynamical magnetic behavior of metal complexes correlates with their phonon modes, which depend on solid polymorphs. However, no systematic study has revealed the correlation between solid phases and spin-lattice relaxation. Herein, we report the magnetism of the VO^{2+}-porphyrinato complex that contains dodecyl chains (**1**). Owing to the flexibility of the molecular structure, we successfully isolated the metastable crystalline phase **1m**, glass phase **1g** and stable crystalline phase **1s**. Although chemical composition of three phases are same, **1s** with the lowest entropy exhibited the longest magnetic relaxation time. Our results suggest that (1) phase stabilization is an effective method for elongating the spin-lattice relaxation time and (2) spin-lattice relaxation correlates with the entropy of the solid.

Introduction

Molecule-based magnetic materials are possible candidates for the components of future information processing/storage devices that utilize the spin degree of freedoms.[1, 2] The magnetic molecules with the strong magnetic anisotropy can behave as the single-molecule magnets (SMMs),[3, 4] which can store 1-bit of information in single molecule as up- or down-spin states: by using SMMs, one can increase the information storage capacity drastically. On the other hand, the magnetic molecules with the negligible magnetic anisotropy are promising as the molecule-based quantum bit (qubit).[5-14] Especially, vanadyl (VO^{2+}) complexes showing isotropic S = 1/2 state undergo long decoherence time (T_2) even at room temperature (T).[5, 15] One of the merits of the molecule-based spin qubit is the facile modification of the ligands based on the rational design, which enables ones to systematically change the distance between electron spins and nuclear spins,[16, 17] packing structures to modulate the vibrational and phonon modes,[18, 19] and also to integrate the spin qubit for construction of multiple qubit.[20]

Elongation of the spin-lattice relaxation time T_1 is required to achieve long T_2 because T_1 is generally longer than T_2. The previous studies for VO^{2+} spin qubit indicated that the suppression of low energy vibrational modes reduces spin-lattice relaxations (and elongates T_1), through which decoherence time (T_2) increases.[18, 21, 22] Therefore, rigid molecular structures, which can be achieved by decreasing the number of atoms, is favored for spin qubit. On the other hand, VO^{2+} complex with long alkyl chains (soft part) is also attractive as it may behave as a spin qubit with a liquid crystalline property. Combination of the liquid crystalline properties with the magnetism can afford the unexpected behavior such as the revers spin crossover,[23] and the facile modulation of the SMM properties upon changing annealing procedure.[24] However, there is no magnetic investigation for VO^{2+} complex with long alkyl chains, presumably due to the conflict of the design criteria to achieve long T_1. Introducing the long alkyl chains gives low melting point and flexible molecular conformations, enabling the isolation of various phases (both crystalline and glass phases) just by changing annealing/crystallization conditions. Especially, the effect of verification on the magnetic relaxation behavior of spin qubit has not yet been fully revealed, and studies have been limited to magnetic molecules in glassy frozen solution mixtures.[25, 26] Thermal conductivity is significantly reduced upon vitrification,[27] inducing the phonon bottleneck (PB) effect due to the delay in heat exchange between the lattice and thermal bath. However, compared to the crystal, the glass shows additional low-energy thermal motions that correlate with the spin-lattice relaxations. If the PB effect is significant compared with the effect of an increased number of low-energy thermal motions, T_1 will elongate upon vitrification. To discuss the effect of low-energy thermal motion, heat capacity measurement is a powerful tool for capturing the vibrational contributions as the entropy (S). Investigations into

[a] The Department of Chemistry, Faculty of Science, Nara Women's University, Nara 6308506, Japan.
[b] Department of Chemistry, Kindai University, 3-4-1 Kowakae, Higashiosaka, Osaka 577-8502, Japan.
[c] Graduate School of Integrated Basic Sciences, Nihon University, 3-25-40 Sakurajosui, Setagaya-ku, Tokyo 156-8550, Japan.
[d] Innovation Research Center for Fuel Cells, The University of Electro-Communications, Chofu, Tokyo 182-8585, Japan.
[e] School of Materials Science and Engineering, Nankai University, Tianjin 300350, China.
[f] , Graduate School of Science, Tohoku University 6-3 Aramaki-Aza-Aoba Aoba-ku, Sendai, Miyagi, 980-8578, Japan.
† Electronic Supplementary Information (ESI) available.

the effect of vitrification and crystal polymorphs on dynamical magnetic properties from the viewpoint of *S* can provide insights for the construction of spin qubits with long relaxation times.

In this work, we report the phase behavior and dynamical magnetic properties for VO^{2+}-porphyrinato complex with the *n*-dodecyl chains (**1**). By changing the crystallization procedure and thermal treatment, we isolated metastable crystalline phase **1m**, glass phase **1g** and stable crystalline phase **1s**. Heat capacity measurements for three phases revealed that **1s** has the lowest entropy. AC magnetic susceptibility measurements revealed that **1m**, **1g** and **1s** exhibited slow magnetic relaxations up to 130 K, which are among the highest *T* values reported for VO^{2+} complexes in solid states.[8] Among three phases, **1g** exhibited shortest T_1, indicating that the vitrification accelerates spin-lattice relaxations in the low dc magnetic field and low *T* regions. In addition, **1s** exhibited longer T_1 than **1m** did, indicating that the stable phase with the lowest entropy is favourable for suppressing spin-lattice relaxations.

Results and Discussion

Synthesis of dodecylated vanadyl-porphyrin and conversion to metastable crystalline phase

1 was synthesized by using base-catalysed ester exchange reaction (Scheme 1). The mixture of VO(TMCPP) (TMCPP = Tetrakis(4-(methoxycarbonyl)phenyl)porphyrinato) and *n*-dodecanol (acting as the reaction solvent and alkoxide source) was stirred at 170 °C in the presence of the catalytic amount of 1,8-diazabicyclo[5.4.0]undec-7-ene (DBU). As the ester exchange reaction among the methoxycarbonyl group and *n*-dodecanol proceeded, the suspension of VO(TMCPP) turned to a solution. This change is an indicative of the formation of **1**, which has high solubility and low melting point compared to VO(TMCPP).

Metastable crystalline phase of **1** (**1m**) was obtained by slow diffusion of dichloromethane solution of **1** into the ethanol. The chemical stability of **1m** was checked by thermogravimetric (TG) and differential thermal analyses (DTA). No significant change in weight was observed upon heating to 573 K, confirming that there was neither solvent inclusion nor chemical decomposition in **1m** (Fig. S6).

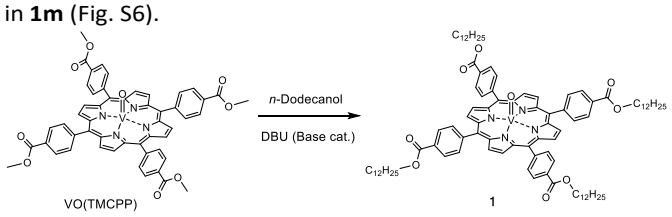

Scheme 1. Reaction scheme for the synthesis of **1**.

Differential scanning calorimetry (DSC)

To check the thermal behaviour of **1m**, DSC measurements were performed at a temperature sweep rate of ±10 K min^{-1} (Fig. S7). No thermal anomaly was observed during the 1st cooling of **1m** from 298 K to 203 K. Upon heating (1st heating), a large endothermic peak ($\Delta_{trs}H$ = 63.1 kJ mol^{-1}) was observed at 364 K. This corresponds to the melting of **1m**, which is consistent with the DTA results (Fig. S6). After melting, no crystallisation or melting was observed. These results indicate that the glassy state (**1g**) was formed by cooling at 10 K min^{-1} after the melting of **1m**.

Heat capacity measurement

For more precise discussion, heat capacity analyses were performed for **1m** using adiabatic calorimetry.[28] In the first heating process from 77 K to 370 K, a broad transition peak was observed at around 180 K (Fig. 1a and 1b up). The transition enthalpy ($\Delta_{trs}H$) and entropy ($\Delta_{trs}S$) were determined to be 3.47 kJ mol^{-1} and 20.3 J K^{-1} mol^{-1}, respectively. A sharp peak was observed at around 360.8 K (Fig. 1a up) which corresponds to melting (Table S2). The cooling (−7 K min^{-1}) of the liquid phase afforded glassy state of the undercooled liquid phase **1g**. On heating **1g**, a small exothermic *T*-drift (+0.01 K h^{-1} at most) and a broad step in heat capacity were observed in the *T* range from 225 to 275 K, implying the glass transition (Fig. S8). Then, **1g** exhibited a clear exothermic *T*-drift (+500 K h^{-1}) above 320 K owing to the crystallization to stable crystalline phase **1s**. In other word, it is possible to convert the metastable crystalline phase **1m** to glass phase **1g** by cooling the melted sample, and to convert stable crystalline phase **1s** by thermal annealing. **1s** showed a sharp peak at 181.8 K, which corresponds to the structural phase transition (Fig. 1a and 1b down). In addition to this sharp peak, broad peak was observed up to 227 K. The $\Delta_{trs}H$ and $\Delta_{trs}S$ was determined to be 9.02 kJ mol^{-1} and 47.9 J K^{-1} mol^{-1}, respectively. Moreover, **1s** exhibited equilibrium transition to **1m** at 354.4 K, and then melted at around 360.8 K. The whole picture of phase relation and thermodynamic stabilities are summarized as a schematic diagram of Gibbs energy against *T* in Fig. S9. To evaluate the degree of disorder, the entropy (*S*) differences of the three phases at 80 K were estimated using C_p data, assuming that the *S* values of the liquid phases obtained from **1m**, **1s** and **1g** were identical (Fig. S10). Among three phases, **1s** exhibited the lowest *S*, and the *S* of **1m** and **1g** were higher by 27.42 J K^{-1} mol^{-1} and 36.10 J K^{-1} mol^{-1} at 80 K,

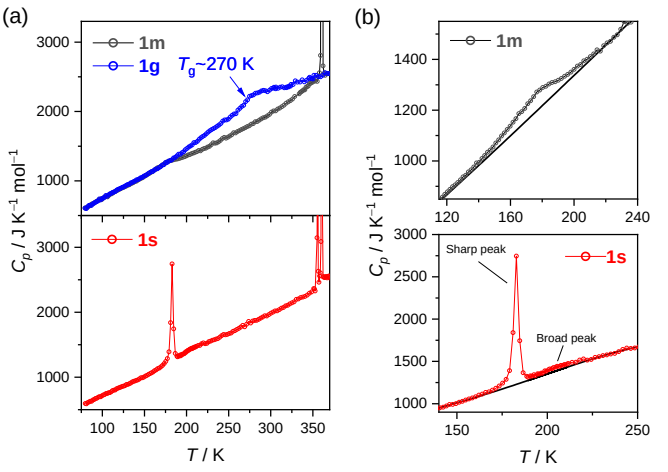

Figure 1. (a) Molar heat capacities for **1m**, **1g** and **1s** obtained using adiabatic calorimetry. (b) Enlarged view of C_p vs. *T* plots of **1m** and **1s** in the vicinity of structural phase transition. Solid lines represent a baseline used for obtaining $\Delta_{trs}H$ and $\Delta_{trs}S$.

respectively. The large *S* value of **1m** compared with that of **1s** indicates the significant contribution of disorders and soft molecular vibration in **1m**.

Single-crystal X-ray diffraction analyses

To reveal correlation between molecular structures and thermal behaviors, we performed single-crystal X-ray diffraction (SCXRD) analyses for **1m** and **1s.** Both crystalline phases exhibited an inversion center at the centroid of porphyrinato core, and adopt VO-up and VO-down conformations (shown as red and blue in Fig. 2, respectively) with 50:50 ratio. The dodecyl chains of **1m** were stretched out from the porphyrinato plane (Fig. 2a), whereas those of **1s** adopted bended and compact conformations, which results in the densely packed structure of **1s** (ρ = 1.203 g cm^{-3} at 153 K) compared with **1m** (ρ = 1.141 g cm^{-3} at 153 K). At 153 K, **1m** exhibited at least three kinds of conformations on dodecyl chains. Compared to **1m**, disorders and thermal factors on dodecyl chains were suppressed in **1s**, wherein only one C-C bond in a dodecyl chain exhibited a positional disorder (Fig. 2b left). The ordered structure of **1s** compared with **1m** is consistent with the low *S* value of **1s** at 80 K. In addition, the large *S* value of **1m** comparable to that of **1g** at 80 K indicates a significant number of low energy excitations associated with dodecyl chains caused by the less densely packed structure of **1m**.

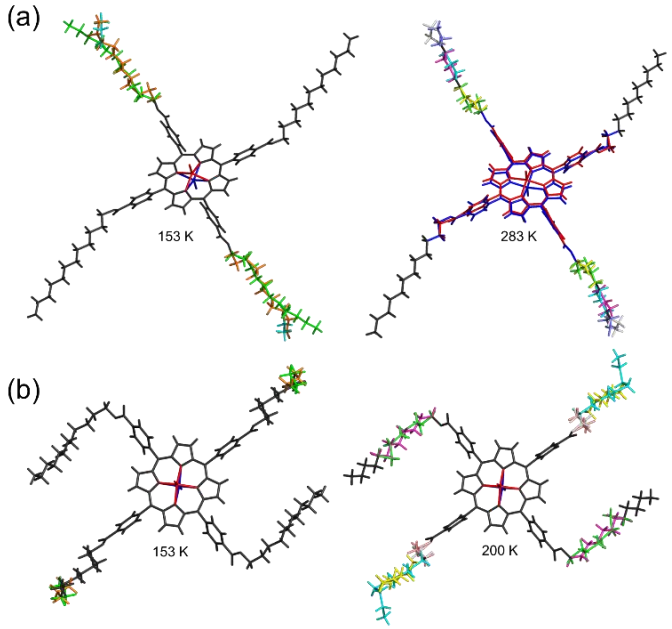

Figure 2. Crystal structures of (a) **1m** and (b) **1s** at 153 K. Disordered structures are depicted in colours.

Structural phase transition of 1m and 1s

Both **1m** and **1s** exhibited structural changes upon elevating *T* (Fig. 2a and 2b left), which are ascribed as the anomalous peaks in C_p below 240 K. In case of **1m**, the porphyrinato core unit superimposed at 153 K, splitted into two positions at 283 K, and the dodecyl chains exhibited heavy disorders. To check the correlation between C_p and crystal structures, *T*-dependence of the crystalline cell parameters for **1m** during cooling and heating process was obtained (Fig. S4). There is no sudden changes in the unit cell parameters upon sweeping *T* (Fig. S4), being consistent with the broad peak in C_p due to gradual structural phase transition over wide *T* range. In case of **1s**, sudden change in unit cell parameters were observed at around 170 K (Fig. S5) in a cooling process and at around 180 K in a heating process due to the structural phase transition with hysteresis behavior. The transition *T* in the heating process matches with the *T* at which C_p peak was observed, confirming that C_p anomaly corresponds to the structural phase transition captured by SCXRD analyses. This phase transition is attributable to the lateral expansion of the molecule due to thermal motion of the dodecyl chains, which was observed as the sudden increase in the number of disordered conformations on dodecyl chains (Fig. 2b right). These conformations became non-visible at 283 K because of the dynamical disorder of the dodecyl chains. Based on the numbers of possible disordered conformations determined from SCXRD analyses, conformational contributions to the $\Delta_{trs}S$ were 16.3 J K^{-1} mol^{-1} for **1m** and 23.1 J K^{-1} mol^{-1} for **1s** (see SI). These values are smaller than the $\Delta_{trs}S$ values obtained by C_p measurements (20.3 J K^{-1} mol^{-1} for **1m** and 47.9 J K^{-1} mol^{-1} for **1s**), indicating the vibrational contribution to the $\Delta_{trs}S$.

Preparation of samples for magnetic measurements

1m for magnetic measurements were prepared by solution diffusion method using dichloromethane and ethanol. **1s** was prepared by keeping the melted **1** at 320 K in the adiabatic calorimeter (see experimental). The phase purity of **1m** and **1s** was checked by powder X-ray diffraction (PXRD) measurements (Figs. S1 and S2). Experimental PXRD patterns of **1m** and **1s** showed good agreement with the ones simulated from SCXRD data, confirming that there was no phase contamination of crystal polymorphs. The glass state **1g** was obtained by rapidly cooling the melted phase by dipping into liquid nitrogen, followed by inserting the sample to the physical property measurement system (PPMS), and then setting the *T* to 150 K with the cooling rate of 20 K min^{-1}. This cooling rate is rapid enough for preparation of **1g**, as proved by C_p measurement and DSC analyses (Fig. S6). In addition, **1g** did not show obvious diffraction peaks (Fig. S3). An extended X-ray absorption fine structure (EXAFS) indicates that coordination geometry VO^{2+} of **1g** is identical to that of **1m** (Fig. S4 and S5).

DC magnetic properties

The VO^{2+} porphyrinato complexes exhibit magnetic properties due to an unpaired electron on non-degenerated d_{xy} orbital; this electronic configuration quenches orbital angular momentum, resulting in the isotropic S = 1/2 spin state. Low spin concentration of the series of **1** makes it difficult to get the reliable magnetic susceptibility above 150 K. Therefore, $\chi_M T$ value of **1m**, **1g** and **1s** under a dc magnetic field of 10 kOe below 150 K was shown in Fig. 3a. $\chi_M T$ value is almost constant above 10 K in all solid phases due to negligible magnetic anisotropy and intermolecular magnetic interactions. Below 10 K, small decrease in $\chi_M T$ value was observed, which is attributable to the weak intermolecular magnetic interactions and magnetization saturation. Curie constants (*C*) determined from fitting the χ_M^{-1} vs. *T* plots in the *T*-rage from 20 to 100 K

were 0.37 cm^3 K mol^{-1} for **1m**, 0.37 cm^3 K mol^{-1} for **1g**, and 0.36 cm^3 K mol^{-1} for **1s**, in good agreement with the value for isotropic S = 1/2 spin with g value of 2 (0.375 cm^3 K mol^{-1}). Magnetization (M) vs. HT^{-1} plots of all phases at 2, 4, 6 and 10 K were overlapped, and reasonably simulated with the Brillouin function with S = 1/2 and g = 2 (Fig. 3b), again confirming the isotropic spin of the **1m**, **1g** and **1s**.

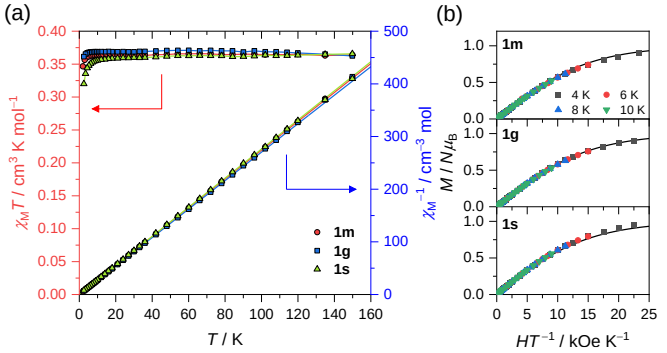

Figure 3. (a) $\chi_M T$ vs. T plots and χ_M^{-1} vs. T plots of **1m**, **1g** and **1s** under a 10 kOe dc magnetic field. Solid lines in χ_M^{-1} vs. T plots represent a fit using Curie's law in the T-range of 20 to 100 K. (b) M vs. HT^{-1} plots at **1m**, **1g** and **1s**. The solid curves represent theoretical M from Brillouin function with S = 1/2 and g = 2.

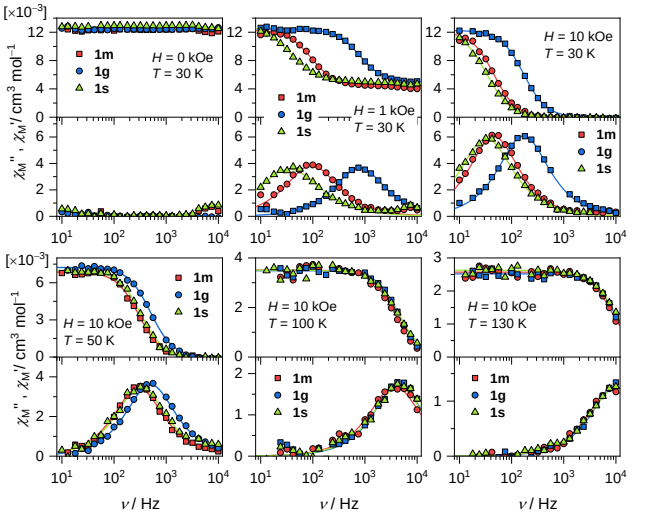

Figure 4. AC magnetic susceptibilities for **1m**, **1g** and **1s** at various H and T. No frequency dependences on χ_M' and χ_M'' were observed at zero H. Solid curves for the plots at non-zero H represent a fit using generalized Debye model.

AC magnetic properties

To investigate the T_1, we performed ac magnetic susceptibility measurements for **1m**, **1g** and **1s** (Fig. 4). Hereafter, we use "τ" instead of T_1 to distinguish the spin-lattice relaxation time obtained by ac measurement (τ) and that by electron paramagnetic resonance (T_1). **1m**, **1g** and **1s** exhibited no ac frequency (ν) dependences on in phase (χ_M') and out-of-phase (χ_M'') of the ac magnetic susceptibilities in the absence of dc magnetic field (upper left of Fig. 4). However, clear slow magnetic relaxation was observed in the presence of non-zero H. At H = 1 kOe and T = 30 K (upper middle of Fig. 4), the χ_M' value at ν = 10^4 Hz was 0.004-0.005 cm^3 mol^{-1} for all phases, indicating that partial amount (ca. 2/3) of the VO^{2+} unit participates the slow magnetic relaxation. At H = 10 kOe however, χ_M' value was almost zero at ν = 10^4 Hz because all amount of the VO^{2+} complex underwent slow magnetic relaxation. With increasing T, the difference in the ac magnetic curves among **1m**, **1g** and **1s** became negligible (Lower raw of Fig. 4), implying that the solid polymorphs affect the dynamic magnetic behaviour at low T as discussed later.

For more precise discussion, τ was obtained by fitting the ac magnetic susceptibilities using generalized Debye model (Figs. S17-22). H dependence of τ at 30 K is summarized in Fig. 5a. Gradual increase in τ values of **1m** and **1g** with increasing H up to 0.4 T corresponds to the quenching of magnetic relaxations mediated by internal magnetic field (magnetic dipole-dipole interactions), which are suppressed by applying dc magnetic field. **1s** did not exhibit such a gradual increase in τ values at the low field, indicating that the magnetic relaxations via internal magnetic field were suppressed. T dependence of τ at a dc magnetic field of 10 kOe (Fig. 5b) of **1g** exhibited small inclination in the low T region and large inclination in the high T region, the boundary of which existed at 30 K. Similar behavior was observed in the τ vs. T plots of **1m**, whereas **1s** did not show changes in inclination in the measured T range. τ vs. T plots of all three phases above 60 K is superimposed. To get the deeper insight into magnetic relaxation, τ vs. H and τ vs. T plots were simulated using the following equation:

$$\tau^{-1} = a_{Dir}H^5 \coth\left(\frac{g\mu_B H}{k_B T}\right) + a_{Ram}T^m + B\frac{1+B_1H^2}{1+B_2H^2}T \qquad \text{Eq. 1}$$

where first and second term represent direct and Raman process, respectively.[29] g-value in the first term is fixed to 1.98, the value typical for VO^{2+} porphyrinato complex.[18] Third one is a Brons-van Vleck term which represents the magnetic relaxation via internal magnetic field.[30] B_1 is the effect of internal magnetic field which induces magnetic relaxation, and B_2 the effect of external magnetic field which quenches internal field, both of which are field and T independent at weak dc magnetic field. Considering that the spin-lattice relaxations via internal field occur with a single phonon, the third term is proportional to T.[13] Orbach process was excluded from the possible relaxation process because there are no available excited states in the measurement T range. In case of **1s**, B was fixed to 0 (As a result, B_1 and B_2 for **1s** were excluded from the optimized parameters) due to negligible H dependence of τ at weak field. In other words, the magnetic relaxations of **1s** in the measured H and T range were driven by direct and Raman processes. In **1m** and **1g**, B_1 and B_2 were expected to be similar due to the lack of the magnetic anisotropy of VO^{2+} ion, making the internal magnetic field of electron spins less dependent on the packing structure. In addition, Raman terms of **1m**, **1g** and **1s** are similar as evidenced by the overlapped τ vs. T plots above 60 K. Therefore, to avoid overparameterization, the optimized parameters for eq. 1 were obtained by using the same Raman term for all phases and sharing the B_1 and B_2 of **1m** and **1g**. H and T dependences on τ were simulated using the optimized parameters summarized in Table 1. The m value of the Raman term is 4.0(1), which is larger but typical range in the reported VO^{2+} complexes.[5, 18, 21] In all case, a_{Dir} values which represent the direct process were similar in magnitude since the τ vs. H plots above 3 T for **1m**-**1s** were similar with each other. In contrast, B values were strongly dependent on the phases. The magnitude

of *B* values correlates with the low energy vibrational modes, which are enhanced in the glass state. Compared to the crystalline phase, glass phase **1g** exhibited larger *B* values. On the contrary, the *B* value of the stable phase **1s** was negligible. Our results suggest that the vitrification accelerates the magnetic relaxations, rather than enhancing PB effect. In contrast, **1s** obtained by phase stabilization exhibited longest τ among three phases. The effect of phases on τ is pronounced at low *T* and low *H*, at which low energy thermal motions accelerate spin-lattice relaxations. These results are consistent with the excess *S* of **1m** and **1g**, which is attributable to the low energy thermal motions of dodecyl chains. In contrast to the low *T* region, τ vs. *T* plots of the three phases above 60 K overlap, indicating that the Raman process in this *T* region correlates with the vibrational mode of the VO(TCPP) core rather than the soft motion of the dodecyl chains.

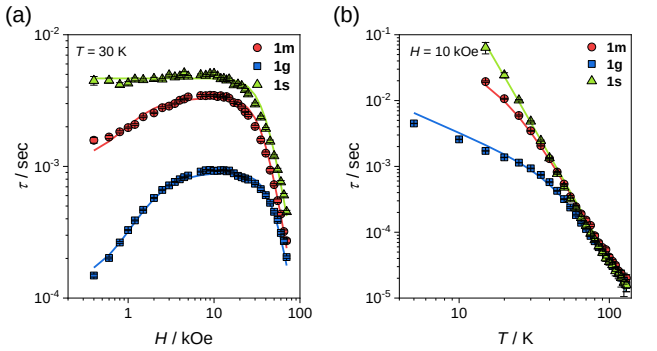

Figure 5. (a) τ vs. *H* (*T* = 30 K) and (b) τ vs. *T* (*H* = 10 kOe) plots at **1m**, **1g** and **1s**. The solid curves represent the fit using Eq. 1.

Table 1. Fitting parameters for **1m**, **1g** and **1s** using eq. 1.

	1m	**1g**	**1s**
a_{Dir} / kOe^{-5} s^{-1}	3.6(4) × 10^{-7}	4.2(7) × 10^{-7}	2.0(2) × 10^{-7}
a_{Ram} / K^{-m} s^{-1}	2.6(8) × 10^{-4}	2.6(8) × 10^{-4}	2.6(8) × 10^{-4}
m	4.0(1)	4.0(1)	4.0(1)
B / K^{-1} s^{-1}	23(6)	2.5(6) × 10^{2}	0 (fixed)
B_1 / kOe^{-2}	0.27(5)	0.27(5)	-
B_2 / kOe^{-2}	2.2(8)	2.2(8)	-

Comparison of magnetic properties with reported analogues

1m and **1s** exhibited long τ values (19-64 ms at 15 K and 15-20 μs at 130 K) compared to the VO(TCPP) (TCPP = tetrakis(4-carboxyphenyl)porphyrinato) analogues (Table 2) [8, 18, 31] even though dodecyl chains act as the source of soft motions. We believe that the elongation of the intermolecular V^{4+}–V^{4+} distances due to the bulkiness of the alkyl chain is the possible explanation for the observed long τ. Magnetic dilution using solution or a diamagnetic crystalline solid matrix elongates the T_1 and T_2 dramatically.[15] The concentration of *S* = 1/2 spin for **1m** and **1s** are 0.45 and 0.47 nm^{-3}, respectively, which are lower than that of ethyl esterified analogue **2** (0.88 nm^{-3}).[8] The τ value of crystalline **2** (ca. 6 ms at 15 K) is shorter than those of **1m** and **1s** (19 and 64 ms at 15 K, respectively) but is longer than that of **1g** (1.7 ms at 15 K). In the case of **1m** and **1s**, the effect of magnetic dilution, which elongates τ, overcomes the effect of soft motion. In the case of **1g**, the effect of soft motion is significant compared to the dilution effect, resulting in the short τ value. The magnetic relaxation times at high *T* seem to be less dependent on magnetic dilution and chemical substitution. T_1 of the frozen solution (0.46 mM, which corresponds to the spin concentration of 2.8 × 10^{-4} nm^3) of **2** (20 μs at 120 K) is comparable to the τ of the present samples (20-24 μs at 120 K). Similar T_1 values have been reported for VO(TCPP)-based 2D[31] and 3D[18] MOFs under dilute conditions (16 μs at 120 K and 22 μs at 100 K, respectively). These independences in T_1 are attributed to the Raman process which is driven by the vibrational motion of the core VO(TCPP) unit.

Table 2. Spin-lattice relaxation time for relevant VO(TCPP) complexes.

	τ, T_1 / μs	*T* / K	DC field / kOe	Concentration / spin nm^{-3}
1m	1.9 × 10^4	15	10	0.45
	24	120		
	20	130		
1g	1.7 × 10^3	15	10	-
	20	120		
	16	130		
1s	6 × 10^4	15	10	0.47
	20	120		
	16	130		
2(crystalline)[8]	6 × 10^{3a}	15	0.05	0.88
2(solution)[8, 32]	20^b	120	3.47	2.8 × 10^{-4}
2DMOF(1%)[31]	16^b	120	3.43	7.4 × 10^{-3}
3DMOF(5%)[18]	22^b	100	3.4	1.3 × 10^{-2}

a: from ac magnetic measurements; b: from EPR measurements

Conclusions

We presented the synthesis and magnetic properties of dodecyl substituted VO^{2+} complex. Slow magnetic relaxations were observed up to 130 K, indicating that introduction of the alkyl chains did not act to decrease T_1. Comparison of dynamical magnetic properties of three phases suggests that the stable phase with low *S* is more promising than metastable phase for suppressing spin-lattice relaxation. To the best of our knowledge, this is the first example that mentions about the relationship between the entropy and spin-lattice relaxations. Our result also suggests the usefulness of heat capacity measurements as the tool for capturing the soft molecular motions as the entropy differences. Heat capacity measurements can capture the contribution of whole vibrational modes, whereas THz spectroscopy used in the previous research[18, 21] cannot capture the vibrational modes which violate a selection rule. Therefore, we believe that heat capacity measurement becomes a powerful tool to reveal the correlation between spin-lattice relaxations and solid polymorphs. To prove the correlation between *S* and dynamic magnetic properties, further investigation for the magnetic relaxation behaviors of various kinds of VO^{2+}-porphyrinato

analogue is needed. Especially, the C_p measurements down to the liquid helium temperature and electron paramagnetic resonance, although not conducted in this research, would be helpful to understand the correlation between soft motion and low temperature spin dynamics including T_2. From the point of view of synthetic chemistry, the use of ester exchange reaction to attach the long alkyl chains can be applied for facile construction of the ligand library. By using this method, we will provide the comprehensive survey which unveils the relationship between phase behavior and spin-lattice relaxation in the future paper.

Experimental

Chemical reagents

Tetrakis(4-methoxycarbonylphenyl)porphyrin (H_2TMCPP) was synthesized according to the literature method.[33] Vanadyl acetylacetonate ($VO(acac)_2$), phenol, and 1,8-diazabicyclo[5.4.0]undec-7-ene (DBU) were purchased from Wako Chemicals. 1-Dodecanol was purchased from Tokyo Chemical Industry. All the reagents were used as received without further purification.

Synthesis of 1m

A mixture of H_2TMCPP (130 mg, 0.15 mmol), $VO(acac)_2$ (102 mg, 0.38 mmol) and phenol (5 mL) was refluxed for 6 hours under N_2. After cooling to room temperature, ca. 30 mL of methanol was added, and the mixture was stirred for ca. 12 h. The violet precipitate was collected by vacuum filtration, washed with methanol, and dried under vacuum. A mixture of the obtained solid, 1-dodecanol (5 mL), and DBU (100 μL) was stirred at 170 °C for 12 h under N_2. After cooling to room temperature, ca. 30 mL of methanol was added and the violet precipitate was collected by vacuum filtration. Silica gel (silica gel 60N, spherical neutral, particle size 100-210 μm) column chromatography, using dichloromethane as the eluent, afforded the main red solution (eluted first) containing **1**. After evaporating the solvent, recrystallisation using dichloromethane/ethanol afforded pure **1m** as red platelet crystals (150 mg, 64% yield). CHN elemental analysis calcd. (%) for $C_{96}H_{124}N_4O_9V$: C 75.41, H 8.17, N 3.66; found: C 75.21, H 8.19, N 3.78.

Preparation of 1s

1s was prepared using an adiabatic calorimeter. **1m** was placed in the adiabatic calorimeter and melted by heating at 400 K. The melted sample was maintained at 320 K, and the temperature (T) drift was monitored. After the complete absence of the exothermic T-drift (took one day), the crystalline sample **1s** was removed from the adiabatic calorimeter.

Crystallization of 1s for SCXRD analyses

A mixture of ca. 1.5 mg of **1m** and 0.5 mL of 1-octanol was heated at 393 K to dissolve **1m** completely. After cooling the mixture to room temperature, a few drops of this solution mixture were added to an excess amount (ca. 0.5 mL) of Paratone-N (Hampton Research). This mixture was maintained at 276 K for ca. 2 weeks to obtain hexagonal-shaped crystals suitable for SCXRD analyses.

Preparation of 1g for magnetic measurements

1m (141 mg) was placed in the gelatine capsule and the capsule was inserted into the straw. After melting **1m** by heating at ca. 390 K using an oven for overnight, the sample was rapidly cooled by dipping the capsule and the straw into liquid nitrogen. The sample was inserted to the physical property measurement system (PPMS) and set the T to 150 K with the cooling rate of 20 K min^{-1}.

Measurements

Single-crystal X-ray diffraction measurements were performed using a Varimax Saturn diffractometer (Rigaku). Diffraction data were processed using CrysAlisPro 4.0. Initial structures were obtained using SHELXT (2018/3) and refined with SHELXL (2018/3)[32] combined with Yadokari-XG.[34] Powder X-ray diffraction patterns were acquired using a D2 Phaser (Bruker). Magnetic measurements were performed using a physical property measurement system (PPMS) equipped with the ACMS option (Quantum Design) and a magnetic property measurement system (MPMS) XL7AC (Quantum Design). The magnetic relaxation time was acquired by fitting the real (χ_M') and imaginary (χ_M') parts of the AC magnetic susceptibilities using the generalised Debye model. Thermogravimetry-differential thermal analysis (TG-DTA) measurement of **1m** was performed using a Rigaku TG8120 instrument. The sample was placed in an aluminum pan and heated from 296 to 573 K at a rate of 10 K min^{-1} under a N_2 atmosphere. DSC data were acquired using a PerkinElmer DSC8500 under a flow of N_2 gas (20 mL min^{-1}). We used aluminum sample pans and covers for all measurements. DSC measurements of **1m** were performed at a heating and cooling rate of 10 K min^{-1} from 203 K to 403 K. Heat capacity measurements were conducted using a homemade adiabatic calorimeter. X-ray absorption spectroscopy was performed at the BL9A High Energy Accelerator Research Organization (KEK) (the edge position was calibrated using that of V foil). The analysis was performed using the Demeter software platform.[35] The crystalline sample (**1m**) for the XASF measurement was prepared by dispersing **1m** in boron nitride (BN) and then pressing into pellets. The melted sample was prepared by melting **1m** inside a plastic bag.

Heat capacity measurements

Heat capacity measurements were conducted at temperatures between 78 and 370 K in the heating direction using a laboratory-made adiabatic calorimeter.[28] The sample was sealed in a vacuum-tight copper cell, whose weight and inner volume were 7302.62 mg and 0.995 cm^3, respectively. Thermal energy was applied in a stepwise manner using a heater wire (ca. 100 Ω) attached to the cell. The amount of energy applied was measured precisely using a source meter (Keithley 2401). The sample temperature was measured using a Rh–Fe alloy resistance thermometer attached to the top of the sample cell. The thermometer was calibrated using an ITS-90 standard. The heat capacity of the empty cell was determined in advance and

subtracted from the total heat capacity to obtain the heat capacity of the sample. The sample weighed 312.44 mg (0.2043 mmol). The contribution of the sample to the total heat capacity was 8.65% in the crystalline phase at 300 K.

Author Contributions

YH: Writing original draft, investigation, data curation, formal analysis, project administration and conceptualization; MM: synthesis of sample, formal analysis, investigation, validation; TY: heat capacity measurement and analysis, preparation of sample, review & editing; ST: formal analysis, review & editing; HS: heat capacity measurement, review & editing, resources; MN: DSC and TG measurements, review & editing; TY: XAFS measurement, review & editing; TK: review & editing, resources; ZYL: review & editing; MY: review & editing, resources, funding sources, project administration and conceptualization.

Conflicts of interest

There are no conflicts to declare.

Acknowledgements

This work was supported by a JSPS KAKENHI grants JP18K14242 (Y. H.), JP19H05631 (M. Y.), JP20K05540 (T. Y.), JP20K15293 (T. K.), JP21K14645 (Y. H.) and the National Natural Science Foundation of China (NSFC, 22150710513). P. M. Y. thanks the support of the 111 project (B18030) from China. This work was performed under the approval of the Photon Factory Program Advisory Committee (Proposal No. 2019G117, beamline 9A).

Notes and references

1. R. Vincent, S. Klyatskaya, M. Ruben, W. Wernsdorfer and F. Balestro, *Nature*, Electronic read-out of a single nuclear spin using a molecular spin transistor. 2012, **488**, 357.
2. A. Gaita-Ariño, F. Luis, S. Hill and E. Coronado, *Nat. Chem.*, Molecular spins for quantum computation. 2019, **11**, 301-309.
3. R. Sessoli, D. Gatteschi, A. Caneschi and M. Novak, *Nature*, Magnetic bistability in a metal-ion cluster. 1993, **365**, 141-143.
4. N. Ishikawa, M. Sugita, T. Ishikawa, S.-y. Koshihara and Y. Kaizu, *J. Am. Chem. Soc.*, Lanthanide Double-Decker Complexes Functioning as Magnets at the Single-Molecular Level. 2003, **125**, 8694-8695.
5. M. Atzori, E. Morra, L. Tesi, A. Albino, M. Chiesa, L. Sorace and R. Sessoli, *J. Am. Chem. Soc.*, Quantum Coherence Times Enhancement in Vanadium(IV)-based Potential Molecular Qubits: the Key Role of the Vanadyl Moiety. 2016, **138**, 11234-11244.
6. M. J. Graham, J. M. Zadrozny, M. S. Fataftah and D. E. Freedman, *Chem. Mater.*, Forging Solid-State Qubit Design Principles in a Molecular Furnace. 2017, **29**, 1885-1897.
7. F. Santanni, A. Albino, M. Atzori, D. Ranieri, E. Salvadori, M. Chiesa, A. Lunghi, A. Bencini, L. Sorace, F. Totti and R. Sessoli, *Inorg. Chem.*, Probing Vibrational Symmetry Effects and Nuclear Spin Economy Principles in Molecular Spin Qubits. 2021, **60**, 140-151.
8. I. Gimeno, A. Urtizberea, J. Román-Roche, D. Zueco, A. Camón, P. J. Alonso, O. Roubeau and F. Luis, *Chem. Sci.*, Broad-band spectroscopy of a vanadyl porphyrin: a model electronuclear spin qudit. 2021, **12**, 5621-5630.
9. K. Chakarawet, M. Atanasov, J. E. Ellis, W. W. Lukens, V. G. Young, R. Chatterjee, F. Neese and J. R. Long, *Inorg. Chem.*, Effect of Spin–Orbit Coupling on Phonon-Mediated Magnetic Relaxation in a Series of Zero-Valent Vanadium, Niobium, and Tantalum Isocyanide Complexes. 2021, **60**, 18553-18560.
10. M. Amoza, L. Maxwell, N. Aliaga-Alcalde, S. Gómez-Coca and E. Ruiz, *Chem. Eur. J.*, Spin-Phonon Coupling and Slow-Magnetic Relaxation in Pristine Ferrocenium. 2021, **27**, 16440-16447.
11. G. Handzlik, M. Magott, M. Arczyński, A. M. Sheveleva, F. Tuna, M. Sarewicz, A. Osyczka, M. Rams, V. Vieru, L. F. Chibotaru and D. Pinkowicz, *J. Phys. Chem. Lett.*, Magnetization Dynamics and Coherent Spin Manipulation of a Propeller Gd(III) Complex with the Smallest Helicene Ligand. 2020, **11**, 1508-1515.
12. C.-Y. Lin, T. Ngendahimana, G. R. Eaton, S. S. Eaton and J. M. Zadrozny, *Chem. Sci.*, Counterion influence on dynamic spin properties in a V(iv) complex. 2019, **10**, 548-555.
13. A. B. Buades, V. S. Arderiu, L. Maxwell, M. Amoza, D. Choquesillo-Lazarte, N. Aliaga-Alcalde, C. Viñas, F. Teixidor and E. Ruiz, *Chem. Commun.*, Slow-spin relaxation of a low-spin $S = 1/2$ FeIII carborane complex. 2019, **55**, 3825-3828.
14. I. Bhowmick, A. J. Roehl, J. R. Neilson, A. K. Rappé and M. P. Shores, *Chem. Sci.*, Slow magnetic relaxation in octahedral low-spin Ni(iii) complexes. 2018, **9**, 6564-6571.
15. M. Atzori, L. Tesi, E. Morra, M. Chiesa, L. Sorace and R. Sessoli, *J. Am. Chem. Soc.*, Room-Temperature Quantum Coherence and Rabi Oscillations in Vanadyl Phthalocyanine: Toward Multifunctional Molecular Spin Qubits. 2016, **138**, 2154-2157.
16. M. J. Graham, C.-J. Yu, M. D. Krzyaniak, M. R. Wasielewski and D. E. Freedman, *J. Am. Chem. Soc.*, Synthetic Approach To Determine the Effect of Nuclear Spin Distance on Electronic Spin Decoherence. 2017, **139**, 3196-3201.
17. C.-J. Yu, M. J. Graham, J. M. Zadrozny, J. Niklas, M. D. Krzyaniak, M. R. Wasielewski, O. G. Poluektov and D. E. Freedman, *J. Am. Chem. Soc.*, Long Coherence Times in Nuclear Spin-Free Vanadyl Qubits. 2016, **138**, 14678-14685.
18. T. Yamabayashi, M. Atzori, L. Tesi, G. Cosquer, F. Santanni, M.-E. Boulon, E. Morra, S. Benci, R. Torre, M. Chiesa, L. Sorace, R. Sessoli and M. Yamashita, *J. Am. Chem. Soc.*, Scaling Up Electronic Spin Qubits into a Three-Dimensional Metal–Organic Framework. 2018, **140**, 12090-12101.

19. M. Yamashita, *Bull. Chem. Soc. Jpn.*, Next Generation Multifunctional Nano-Science of Advanced Metal Complexes with Quantum Effect and Nonlinearity. 2021, **94**, 209-264.
20. J. Ferrando-Soria, Samantha A. Magee, A. Chiesa, S. Carretta, P. Santini, Iñigo J. Vitorica-Yrezabal, F. Tuna, George F. S. Whitehead, S. Sproules, Kyle M. Lancaster, A.-L. Barra, Grigore A. Timco, Eric J. L. McInnes and Richard E. P. Winpenny, *Chem. Eur. J.*, Switchable Interaction in Molecular Double Qubits. 2016, **1**, 727-752.
21. M. Atzori, L. Tesi, S. Benci, A. Lunghi, R. Righini, A. Taschin, R. Torre, L. Sorace and R. Sessoli, *J. Am. Chem. Soc.*, Spin Dynamics and Low Energy Vibrations: Insights from Vanadyl-Based Potential Molecular Qubits. 2017, **139**, 4338-4341.
22. M. Atzori, S. Benci, E. Morra, L. Tesi, M. Chiesa, R. Torre, L. Sorace and R. Sessoli, *Inorg. Chem.*, Structural Effects on the Spin Dynamics of Potential Molecular Qubits. 2018, **57**, 731-740.
23. S. Hayami, Y. Shigeyoshi, M. Akita, K. Inoue, K. Kato, K. Osaka, M. Takata, R. Kawajiri, T. Mitani and Y. Maeda, *Angew. Chem. Int. Ed.*, Reverse Spin Transition Triggered by a Structural Phase Transition. 2005, **44**, 4899-4903.
24. M. Gonidec, F. Luis, A. Vilchez, J. Esquena, D. B. Amabilino and J. Veciana, *Angew. Chem. Int. Ed.*, A liquid-crystalline single-molecule magnet with variable magnetic properties. 2010, **49**, 1623-1626.
25. A. J. Fielding, S. Fox, G. L. Millhauser, M. Chattopadhyay, P. M. H. Kroneck, G. Fritz, G. R. Eaton and S. S. Eaton, *J. Magn. Reson.*, Electron spin relaxation of copper(II) complexes in glassy solution between 10 and 120 K. 2006, **179**, 92-104.
26. J. L. Du, G. R. Eaton and S. S. Eaton, *Appl. Magn. Reson.*, Effect of molecular motion on electron spin phase memory times for copper(II) complexes in doped solids. 1994, **6**, 373-378.
27. R. C. Zeller and R. O. Pohl, *Phys. Rev. B*, Thermal Conductivity and Specific Heat of Noncrystalline Solids. 1971, **4**, 2029-2041.
28. A. Inaba, H. Suzuki, M. Massalska-arodź and T. Rozwadowski, *J. Chem. Thermodyn.*, Polymorphism and thermodynamic functions of liquid crystalline material 4-cyano-3-fluorophenyl 4-butylbenzoate. 2012, **54**, 204-210.
29. A. Abragam and B. Bleaney, *Electron paramagnetic resonance of transition ions*, OUP Oxford, 2012.
30. A. C. De Vroomen, E. E. Lijphart, D. Y. H. Prins, J. Marks and N. J. Poulis, *Physica*, Electron spin-lattice relaxation of the Zeeman and interaction systems in $CuCs_2(SO_4)_2{\cdot}6H_2O$. 1972, **61**, 241-249.
31. A. Urtizberea, E. Natividad, P. J. Alonso, L. Pérez-Martínez, M. A. Andrés, I. Gascón, I. Gimeno, F. Luis and O. Roubeau, *Mater. Horiz.*, Vanadyl spin qubit 2D arrays and their integration on superconducting resonators. 2020, **7**, 885-897.
32. G. Sheldrick, *Acta Crystallogr. A*, A short history of SHELX. 2008, **64**, 112-122.
33. D. Feng, W.-C. Chung, Z. Wei, Z.-Y. Gu, H.-L. Jiang, Y.-P. Chen, D. J. Darensbourg and H.-C. Zhou, *J. Am. Chem. Soc.*, Construction of Ultrastable Porphyrin Zr Metal–Organic Frameworks through Linker Elimination. 2013, **135**, 17105-17110.
34. C. Kabuto, S. Akine, T. Nemoto and E. Kwon, *Nihon Kessho Gakkaishi*, Release of Software (Yadokari-XG 2009) for Crystal Structure Analyses. 2009, **51**, 218-224.
35. B. Ravel and M. Newville, *J. Synchrotron Radiat.*, ATHENA, ARTEMIS, HEPHAESTUS: data analysis for X-ray absorption spectroscopy using IFEFFIT. 2005, **12**, 537-541.